Chemical Science

EDGE ARTICLE

View Article Online
View Journal | View Issue

Check for updates

Cite this: *Chem. Sci.*, 2018, **9**, 1902

A simple multi-responsive system based on aldehyde functionalized amino-boranes†

Yong-gang Shi,[a] Jun-wei Wang,[a] Haijun Li,[b] Guo-fei Hu,[a] Xue Li,[a] Soren K. Mellerup,[b] Nan Wang,[a] Tai Peng*[a] and Suning Wang *[ab]

Received 17th August 2017
Accepted 2nd January 2018

DOI: 10.1039/c7sc03617e

rsc.li/chemical-science

A simple aldehyde functionalized amino-triarylborane donor–acceptor system (**BO-1**) was found to display distinct responses toward multiple external stimuli including solvent, temperature and pressure, with emission colours changing from blue to red. The operating mechanism most likely involves reversible switching between closed and open structures based on an intramolecular B ← O bond. Imbedded donor–acceptor charge transfer transitions played a key role in the multi-coloured fluorescent response of this new boron system to external stimuli. Multi-coloured and erasable fluorescent images on solid substrates based **BO-1**'s "turn-on" response toward solvents, particularly water, are demonstrated.

Open Access Article. Published on 04 January 2018. Downloaded on 28/07/2024 1:37:06 AM.
This article is licensed under a Creative Commons Attribution-NonCommercial 3.0 Unported Licence.

Introduction

Multi-responsive systems are highly attractive and important because of their potential applications in a variety of sensing and monitoring/tracking technologies.[1] Many previously reported stimuli-responsive systems are based on transition-metal compounds, some of which display highly sensitive and robust responses toward external stimuli such as light,[1a,2] pressure,[1a–d,3] temperature,[1a,e,4] and oxygen,[1a,5] *etc.* Main-group based responsive systems are more appealing because of their low cost. As a result, main-group systems that respond to external stimuli have attracted much attention recently and many interesting examples have been reported.[6–8] Nonetheless, multi-responsive main-group based systems remain rare and underexplored. Organoboron-based systems have recently been demonstrated to be very promising as responsive materials.[6,7] Although the operating mechanisms of some of the boron-based responsive systems are often similar to those observed in other organic π-conjugated materials or transition metal based systems such as changes in molecular aggregation/intermolecular interactions or fluorescence to phosphorescence switching,[7,8] recent studies have shown that boron-based responsive systems do have a few unique features for achieving responses to external stimuli. For example, the responsive properties of boron compounds could be modulated by the following: (a) reversible B ← X bond formation/cleavage,[6a–d] (b) donor–acceptor charge transfer (CT) transition modulation,[6e,f] (c) reversible B–C/C–C bond formation/cleavage, *etc.*,[6g–k] and (d) visible light induced *E*/*Z* isomerization.[6c,d,l] Recently reported organoboron-based responsive systems typically rely on/address one of these features. Donor–acceptor systems have a special place in organoboron chemistry and organoboron-based optoelectronic materials.[9] Manipulating donor–acceptor interactions in boron-based systems has led to non-linear optical materials,[10] anion sensors,[11] charge transport materials for solar cells,[12] emitters for organic light emitting devices (OLEDs),[13] and molecular thermometers.[6e,f] Combining a switchable internal donor–acceptor bond with an internal donor–acceptor CT system could allow the creation of new and versatile multi-responsive materials. However, to the best of our knowledge, this strategy has not yet been explored for multi-responsive systems. Furthermore, for practical applications, it is always desirable to have a simple system that is easy and cheap to produce. Based on these considerations and inspired by the recent advances in boron-based responsive materials, we designed and investigated simple responsive boron systems, depicted in Scheme 1.

Two key features are implemented in the new molecules we designed. The first feature is the inclusion of a potentially switchable B ← O unit. In order to achieve reversible boron–donor (L) bond switching, the B–L bond must be relatively weak, which could be achieved by either enhancing steric congestion around the boron centre, introducing a weak donor, or reducing the electrophilicity of the boron atom. Thus, to ensure a weak B–L bond, the bulky mesityl groups were chosen for the aryl substituents on boron, which also protect the boron centre from nucleophilic attack by external donors such as water or solvent molecules. In addition, an aldehyde group was chosen as the donor for binding to boron because it is a relatively weak donor, as indicated by the ^{11}B chemical shift of the previously reported

[a]*Key Laboratory of Cluster Science, Ministry of Education, Beijing Key Laboratory of Photoelectronic/Electrophotonic Conversion Materials, School of Chemistry and Chemical Engineering, Beijing Institute of Technology of China, Beijing, 102488, People's Republic of China. E-mail: pengtai@bit.edu.cn*

[b]*Department of Chemistry, Queen's University, Kingston, Ontario, K7L 3N6, Canada. E-mail: sw17@queensu.ca*

† Electronic supplementary information (ESI) available. CCDC 1568989, 1568988, 1569175 and 1585930. For ESI and crystallographic data in CIF or other electronic format see DOI: 10.1039/c7sc03617e

This journal is © The Royal Society of Chemistry 2018

Open Access Article. Published on 04 January 2018. Downloaded on 28/07/2024 1:37:06 AM.
This article is licensed under a Creative Commons Attribution-NonCommercial 3.0 Unported Licence.

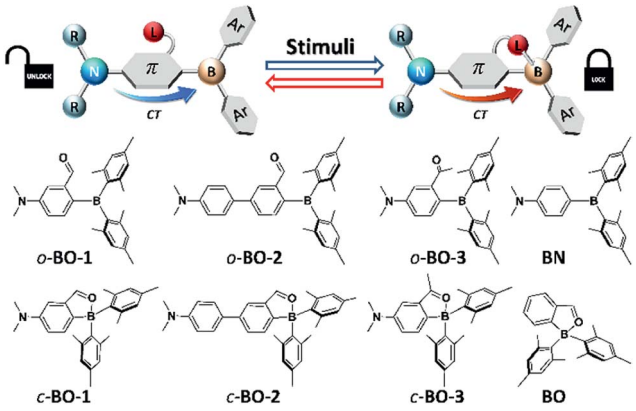

Scheme 1 The main operating mechanism and the structures of the newly designed donor–acceptor boron compounds and control compounds for the study of multi-responsive systems.

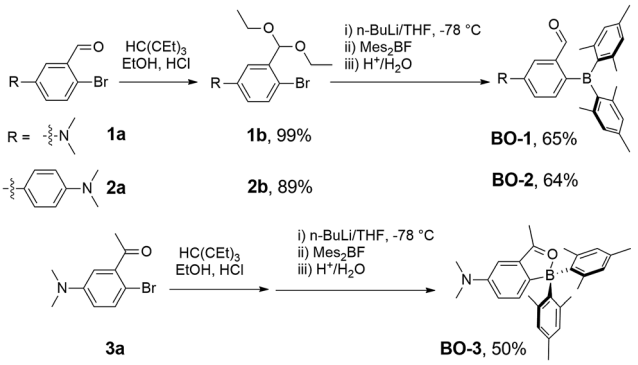

Scheme 2 Synthetic procedures for BO1, BO-2 and BO-3.

compound **BO** at 25 ppm (compared to the corresponding imine analogue that has a ^{11}B chemical shift of 5 ppm).[14] The second feature is the installation of an NMe_2 donor unit, which is well known to produce strong intramolecular charge transfer (ICT) transitions when combined with a triarylboron.[9,10] Furthermore, the amino group allows the modulation of the electron density/electrophilicity of the boron centre. Two different linkers, phenyl and biphenyl, were included in the structural design of molecules **BO-1** and **BO-2** to further modulate the ICT and the B–O bond strength. The previously reported compounds, **BO** and[10a,b] **BN**, and a new compound **BO-3** in which the aldehyde group is replaced by a ketone group, were also examined as control compounds for this work. We have found that molecule **BO-1** responds to both pressure and temperature, while **BO-2** and **BO-3** either respond only to temperature, or have no response to temperature and pressure, due to their distinct difference in structures. In addition, **BO-1** displays distinct "turn-on" fluorescence colour changes on solid substrates upon exposure to different solvent molecules, including water, enabling the use of this molecule for simple fluorescent patterning/writing with solvents. The details of this work are presented herein.

Results and discussion

Synthesis and crystal structures

Compounds **BO-1**, **BO-2** and **BO-3** were obtained according to the procedure shown in Scheme 2. The starting materials **1a** and **3a** were prepared according to a literature procedure[15] and the synthetic details for **2a** are provided in the ESI.† After protecting the carbonyl group in **1a–3a** with the ethoxy group, the $BMes_2$ unit can be attached to the benzene ring *via* lithiation and substitution, producing **BO-1–BO-3** in good yields. Because the intermediate **3b** for **BO-3** is unstable, it was not isolated. All three compounds were fully characterized by NMR, HRMS and single-crystal X-ray diffraction analyses. $^{11}B\{^1H\}$ NMR spectra indicated that these three compounds have distinct structures. In C_6D_6, the ^{11}B chemical shift of **BO-1** appears at 60 ppm, while that of **BO-2** and **BO-3** is at 30 ppm and 16 ppm, respectively. Compared to **BO** that has a ^{11}B signal at 25 ppm, **BO-2** and **BO-3** likely have the closed structures shown in Scheme 1, while **BO-1** likely has the open structure. The much upfield shifted ^{11}B signal of **BO-3** indicates that it has a stronger B–O bond than that of **BO-2**.

This was confirmed by crystallographic analyses. As shown in Fig. 1, **BO-1** has a typical three-coordinate boron centre, while **BO-2** and **BO-3** have a tetrahedral boron centre with B–O bond length of 1.645(2) Å, and 1.626(3) Å, respectively (the B–O bond length in **BO** is 1.641(2) Å). The B–C_{Mes} bond lengths in **BO-2**/**BO-3** (1.636(3), 1.637(3) Å for **BO-2**; 1.640(4), 1.642(3) Å for **BO-3**) are much longer than those in **BO-1** (1.574(2), 1.570(2) Å), consistent with the more congested boron centre in **BO-2**/**BO-3**. The crystals/crystalline powders of **BO-1** and **BO-2**/**BO-3** have distinct colours in the crystalline state – yellow and red-orange, respectively, as shown in Fig. 1, which is clearly a consequence of their distinct structures. **BO-1** forms an extended 1D structure in the crystal lattice *via* H bonds between the oxygen atom and the H atoms of the NMe_2 unit. The fact that **BO-1** has the open form can be attributed to the zwitterionic resonance structure shown in Fig. 1, which greatly reduces the electrophilicity of the boron center toward the oxygen atom. For the biphenyl linked **BO-2** molecule, the zwitterion resonance structure is less important since it involves the dearomatization of two phenyl rings. As a result, the B center in **BO-2** is more electrophilic and capable of forming the chelate structure. The electron donating and bulky methyl group in **BO-3** is clearly responsible for the formation of the closed form. Efforts to obtain the closed form of **BO-1** by using/mixing different solvents such as CH_2Cl_2, CH_3CN, methanol, water, *etc.* in the crystallization process inevitably led to the formation of the *o*-**BO-1** crystals that consistently display the same colour and the same unit cell parameters. All three compounds are stable for months under ambient conditions in solution and in the solid state (see Fig. S35†).

Distinct photophysical properties of BO-1–BO-3

As shown in Fig. 2, the absorption spectrum of **BO-1** is distinctly different from those of **BO-2**/**BO-3**, with a strong absorption band at ~400 nm that could be assigned to the amino to boron/carbonyl ICT transition. A weak absorption band at ~400 nm in

Open Access Article. Published on 04 January 2018. Downloaded on 28/07/2024 1:37:06 AM.
This article is licensed under a Creative Commons Attribution-NonCommercial 3.0 Unported Licence.

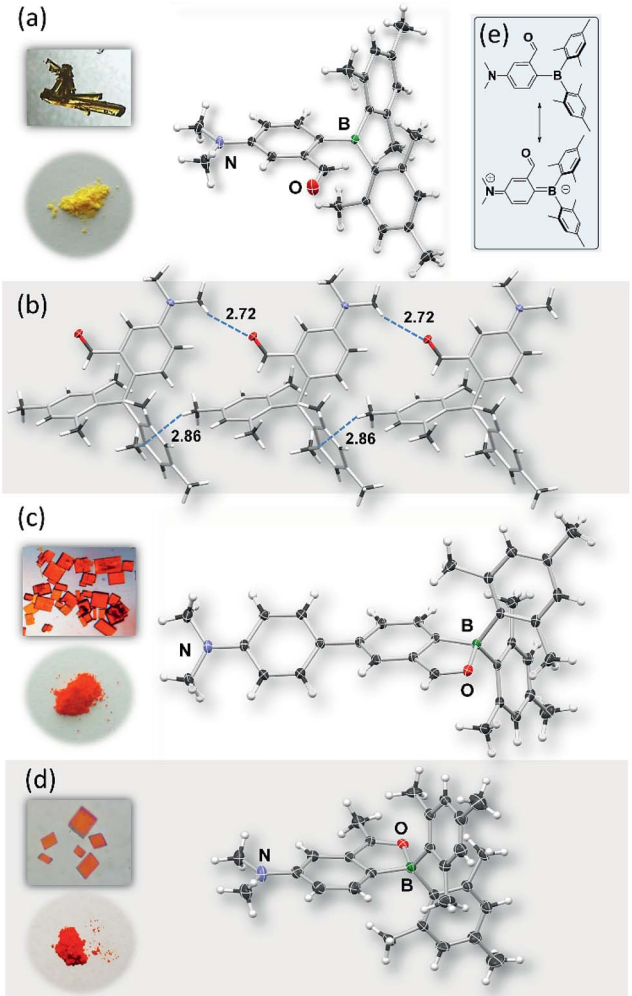

Fig. 1 Crystal structures of **BO-1** (a), **BO-2** (c) and **BO-3** (d) with 35% thermal ellipsoids, the inset photographs show the colours of crystals and powders of **BO-1**, **BO-2** and **BO-3**, respectively. (b) The packing diagram of **BO-1** showing intermolecular H-bonds. (e) The two resonance forms of **BO-1**.

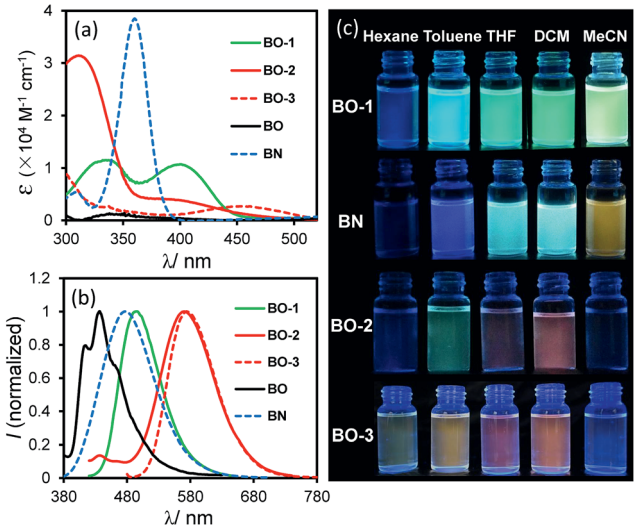

Fig. 2 Absorption (a) and fluorescence spectra (b) (recorded with $\lambda_{ex} = \lambda_{max}$ of the first low energy absorption band) of **BO-1**, **BO-2**, **BO-3**, **BO** and **BN** in CH_2Cl_2 (0.01 mM). (c) Photographs showing fluorescent colours of **BO-1**, **BO-2**, **BO-3** and **BN** in selected solvents (0.01 mM). Photos of **BO** can be found in ESI.†

the spectrum of **BO-2** agrees with its closed structure shown by the crystal structure, which diminishes the ICT transitions. In addition, the absorption tail of **BO-2** stretches further to the longer wavelength than that of **BO-1** (CH_2Cl_2, 0.01 mM). **BO-3** has a distinct absorption band at 450 nm. At 0.10 mM, **BO-1** has a weak, but distinct low energy band at about 450 nm, resembling that of **BO-3** (see Fig. 2 and ESI†). For comparison, the absorption spectra of **BN** and **BO** compounds are also included in Fig. 2. The ICT transition band of **BN** appears at a much higher energy and is more intense than those of **BO-1** and **BO-2**/**BO-3**, while **BO** has only very weak absorption bands in the near UV region. This illustrates the dramatic impact on the electronic properties of the boron compounds induced by a subtle change in the structure or the introduction of a 2nd donor group. In the fluorescence spectra (CH_2Cl_2, 0.01 mM, 298 K), the emission peak of **BO-2**/**BO-3** appears at 584 nm/591 nm, nearly 100 nm bathochromically shifted relative to that of **BO-1** (490 nm). As a result, **BO-1** displays a blue-green emission colour, while **BO-2** and **BO-3** have a pinkish red/red-orange colour in CH_2Cl_2. In addition to the emission colour difference, the emission quantum efficiency also varies sharply, with Φ_{FL} = 0.61, 0.25, 0.45 in CH_2Cl_2, for **BO-1**, **BO-2**, and **BO-3**, respectively (see Table 1). Furthermore, the emission λ_{max} and colour of **BO-1**, **BO-2** and **BO-3** have a distinct dependence on solvent polarity as shown in Fig. 2 (see ESI†). For **BO-1**, its solvent-dependent emission resembles that of **BN**, which, along with its high Φ_{FL}, further supports the strong N to B/C=O ICT character in **BO-1**. **BO-2** and **BO-3** also display solvent dependent emission, although the emission spectral shift with solvent polarity is much less for **BO-3**. **BO-2** is essentially non-emissive in DMF/CH_3CN.

To elucidate the origin of electronic transitions that are responsible for the distinct photophysical properties of molecules **BO-1** and **BO-2**/**BO-3**, TD-DFT computational studies at the B3LYP/6-31g(d) level of theory were performed for both open and closed forms of **BO-1**/**BO-2**, and the closed form of **BO-3**, and the following findings were obtained. For the closed forms, the $S_0 \rightarrow S_1$ vertical excitation involves mainly HOMO to LUMO transitions (92% and 82%, for **BO-1** and **BO-2**, respectively) at 523 nm (**BO-1**) and 532 nm (**BO-2**) with weak oscillator strength. The HOMO orbital of closed **BO-1** and **BO-2**/**BO-3** involves mainly a Mes and NMe_2-Ph (**BO-1**/**BO-3**) or NMe_2-Ph (**BO-2**), while the LUMO orbital involves the B,O-Ph chelate (see Fig. 3). Therefore, the $S_0 \rightarrow S_1$ transitions for the closed molecules have some CT character. The emission peak at 584 nm/591 nm for **BO-2**/**BO-3** can be attributed to the $S_1 \rightarrow S_0$ transition of the closed form. For the open form, the $S_0 \rightarrow S_1$ transition for both **BO-1** and **BO-2** is a CT transition involving HOMO and LUMO orbitals, located on the NMe_2 and the Ar linker, and the boron-benzaldehyde, respectively, with very high oscillator strength as shown in Fig. 3. The weak absorption band of **BO-1** at 450 nm is

This journal is © The Royal Society of Chemistry 2018

Open Access Article. Published on 04 January 2018. Downloaded on 28/07/2024 1:37:06 AM.
This article is licensed under a Creative Commons Attribution-NonCommercial 3.0 Unported Licence.

Table 1 Photophysical data for compounds BO-1–BO-3

	Absorption (nm)	Emission, 298 K			Emission, 77 K
		CH_2Cl_2 (0.1 mM)	Unground powder	Ground powder	CH_2Cl_2 (0.1 mM)
Compounds	CH_2Cl_2 (0.1 mM)	λ_{max} [nm], τ (ns), Φ_{FL}[a]	λ_{max} [nm], τ (ns), Φ_{FL}[a]	λ_{max} [nm], τ (ns), Φ_{FL}[a]	λ_{max} [nm], τ (ns), Φ_{FL}[a]
BO-1	400	499, 14.1, 0.61	473, 2.9, 0.07 600, 9.1, 0.06	465, 1.5, 0.001 620, 6.1, 0.05	468, 8.9, 0.04 604, 13.5, 0.09
BO-2	400	584, 6.3, 0.25	611, 8.7, 0.10	N/A	606, 28.2, 0.11
BO-3	454	591, 30, 0.45	628, 8.0, 0.11	N/A	574, 44, 0.56

[a] Determined using an absolute QY spectrometer.

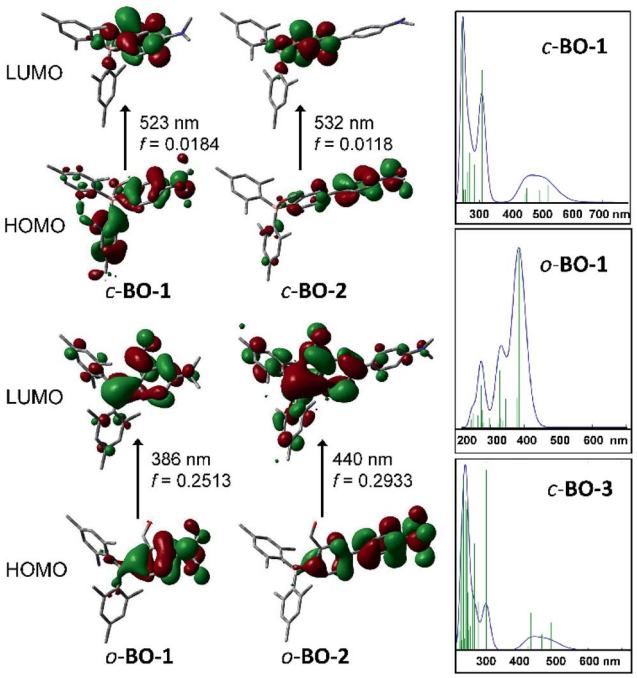

Fig. 3 HOMO and LUMO diagrams of BO-1 and BO-2 and TD-DFT (B3LYP/6-31g(d)) calculated absorption spectra of *c*-BO-1/*o*-BO-1 and *c*-BO-3.

clearly not from the open form, based on TD-DFT data. The $S_0 \rightarrow S_1$ transition energy of ***o*-BO-1** is blue shifted about 100 nm, compared to that of ***c*-BO-1**. Based on the experimentally observed and the TD-DFT calculated absorption spectra (see ESI†), the distinct emission colour of **BO-1** and **BO-2**/**BO-3** is most likely caused by their preferential adoption of the open and the closed forms, respectively. The strongly solvent-dependent fluorescence of **BO-1** agrees with the strong ICT character of the open form. The low emission quantum efficiency of **BO-2** can be attributed to the low oscillator strength of the $S_0 \rightarrow S_1$ transition in ***c*-BO-2**. For ***c*-BO-3**, the $S_0 \rightarrow S_1$ transition oscillator strength (0.0207) is much greater than that of ***c*-BO-2**, thus leading to a brighter emission. Electrochemical analysis shows that the reduction potential of the aldehyde group in **BO-1** is 0.25 V more positive than that of **BO-2**, which agrees with the DFT calculated LUMO energies of the ***o*-BO-1** and the ***c*-BO-2**. Similarly, the oxidation potential of the amino group in **BO-1** is ~0.29 V more positive than that of **BO-2**, which also agrees with the calculated HOMO energy difference of ***o*-BO-1** and the ***c*-BO-2** (see Fig. S46, Tables S8 and S9†). DFT data indicate that in the gas phase, the ***o*-BO-1** is slightly more stable than ***c*-BO-1** (by about 0.8 kcal mol^{-1}) and the activation barrier from the ***o*-BO-1** to ***c*-BO-1** is less than 7 kcal mol^{-1} (see Fig. S50†). It is therefore reasonable to suggest that in solution and at ambient temperature, ***o*-BO-1** and ***c*-BO-1** are likely in equilibrium, with ***o*-BO-1** being the dominating form.

Distinct impact of water on the emission colour of BO-1 and creating fluorescent paintings with solvents as ink

Among all the solvents we examined for **BO-1**, water was found to have a unique impact on the emission colour of **BO-1**. In either CH_3CN or THF (see Fig. S26–S28†), the emission colour of the **BO-1** solution changes gradually from blue green to green in THF, and green to whitish yellow in CH_3CN with increasing water content, accompanied by a sharp decrease in Φ_{FL} (*e.g.* from 0.45 in THF to 0.02 in a 70% water solution). When the water content exceeds 70%, the emission colour of the solution experiences a sharp change to red-orange, with an emission peak appearing at ~605 nm, as shown in Fig. 4. Accompanying this is the distinct increasing of an absorption band at about 500 nm, which decreases a bit at 92% water level, due perhaps to a small amount of precipitate formation. The red emission peak of **BO-1** in a mostly water solution resembles that of ***c*-BO-2** (see Fig. S17†), except that the ***c*-BO-2** emission in such a solution is extremely weak (Φ_{FL} < 0.001) (***c*-BO-3** becomes insoluble).

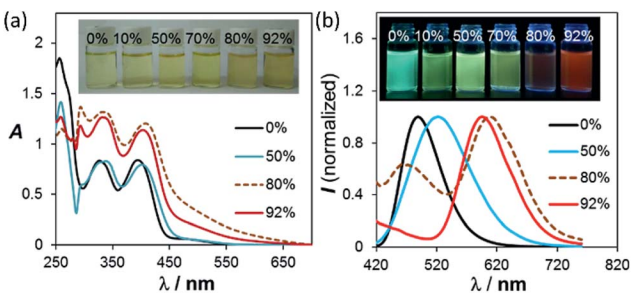

Fig. 4 (a) Changes in the absorption and (b) fluorescence spectra of BO-1 in THF (1×10^{-4} M), with increasing water content. For the complete spectra, see ESI.†

Open Access Article. Published on 04 January 2018. Downloaded on 28/07/2024 1:37:06 AM.
This article is licensed under a Creative Commons Attribution-NonCommercial 3.0 Unported Licence.

The emission peak of **BO-2** experiences about a 35 nm bathochromic shift from THF to water (~95%), while that of **BO-1** has about 105 nm bathochromic shift. In contrast, the addition of water to the THF or CH_3CN solution of **BN** shifts the emission band hypsochromically (~60 nm from THF to 92% water, ~90 nm from CH_3CN to 92% water) with either increased Φ_{FL} or little Φ_{FL} change (see Fig. S25b†), which may be caused by aggregation induced structural rigidification and the highly hydrophobic nature of **BN**. TD-DFT calculations for *o*-**BO-1** using water as the dielectric medium show that the amino group becomes pyramidal and the dihedral angle between the planes of phenyl and NMe_2 increases from 11° to 27°, accompanied by a 30 nm red shift of the $S_0 \rightarrow S_1$ vertical excitation energy (30 nm) with a very high oscillator strength (0.1990), compared to that in the gas phase (see ESI†), owing to the twisted ICT (TICT) effect.[16] Because of the very low absorbance of the absorption band of **BO-1** at 450 nm, it cannot be attributed to *o*-**BO-1** in water. Water molecules likely interact with the amino group in *o*-**BO-1**, reducing its donating ability to the boron centre *via* TICT, thus increasing the electrophilicity of the boron center and facilitating the formation of the closed structure. The oxygen atom of the water molecules may also interact with the carbonyl group in *o*-**BO-1**, enhancing the nucleophilicity of the oxygen atom,[17] allowing it to form a B–O bond. Addition of fluoride ions to **BO-1** led to a distinct fluorescence quenching without colour change (see ESI†). Hence, the red emission colour of **BO-1** in the presence of water is not caused by water binding to the boron centre. Definitive evidence for the formation of *c*-**BO-1** in the presence of water was obtained from the ^{11}B NMR spectra, which showed that the ^{11}B peak of **BO-1** shifts from 58 ppm in THF to ~0 ppm in the 4 : 1 solvent mixture of water and THF (see Fig. S16a†), thus unequivocally establishing that **BO-1** has a closed structure in the presence of water. The water induced change in **BO-1** is fully reversible upon the addition of organic solvents.

Although Φ_{FL} (0.03 in 92% water + THF and 0.04 in 98% water + CH_3CN) of **BO-1** in water is much lower than that in THF (0.45) or CH_3CN (0.58), the emission colour is readily visible. Most interesting is the finding that the solvent/water-dependent emission colour of **BO-1** can also be visualized on solid substrates such as silica gel thin-layer chromatography (TLC) plates. One example is shown in Fig. 5(a). In this demonstration, three letters were written on a TLC plate using 1.3 mM CH_2Cl_2 solution of **BO-1**. After the solvent is evaporated, under UV light illumination, the three letters display the characteristic blue-green emission colour of **BO-1**. As the letters are wet with drops of water, the emission colour switches immediately to red-orange. After the TLC plate is dried to remove the water, the emission colour reverts to blue-green. Fluorescence spectra indicate that this is a fully reversible process (see Fig. S27†), supporting that the water induced structural transformation of **BO-1** can occur reversibly on silica gel support. Addition of water to **BO-1** crystals/powder does not change the emission colour, perhaps due to the high crystal lattice energy. The second example is shown in Fig. 5(b) and (d). In this example, the TLC plate was first treated with a 0.1 mM CH_2Cl_2 solution of **BO-1** and then dried. Under UV illumination

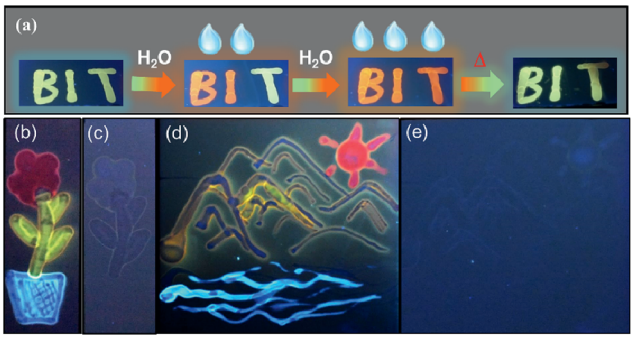

Fig. 5 (a) Photographs showing the reversible emission colour change of letters written on a pristine TLC plate (with a 1.3 mM CH_2Cl_2 solution of **BO-1**) with water and heating. (b and d) Photographs showing paintings created using a cotton tip and selected solvents as inks on a TLC plate treated with a **BO-1** solution (CH_2Cl_2, 0.1 mM). Water: red; DMF: yellow; toluene: blue. A handheld UV lamp (365 nm) was used to illuminate the images created. (c and e) Photographs showing the disappearance of the images after the TLC plate is dried at rt.

(365 nm), such treated TLC plates appear dark with very weak blue emission. Next, a small cotton swab, soaked with a selected solvent (pure solvent) was used to draw pictures on the plate. In order to provide sufficient time for the camera to capture the images created, high boiling point solvents such as DMF, toluene and water were used. These three solvents also provide distinct emission colours to the image – DMF: yellow-green, toluene: blue, water: red. Images created in such manner vanish as the ink/solvent evaporates, as shown by Fig. 5(c) and (e). The TLC plates can be reused for creating new images. This "solvent-turn on" emission effect of **BO-1** on a TLC plate may be attributed to the large emission quantum efficiency difference of **BO-1** in solution and in the solid state (*e.g.* $\Phi_{FL} = 0.61$ in CH_2Cl_2; 0.45 in 2-methoxyethyl ether (MOE); 0.15 in crystalline powder). Similar effects cannot be achieved for **BO-2**/**BO-3** because of the similar and low Φ_{FL} in both solution and solid states (*e.g.* $\Phi_{FL} = 0.25$ in CH_2Cl_2; 0.09 in MOE, 0.10 as crystalline powder) for **BO-2**, and the small emission colour change of **BO-3** in different solvents. For the **BN** compound, it has a very high Φ_{FL} in both solution and the solid state (*e.g.* $\Phi_{FL} = 0.71$ in CH_2Cl_2; 0.57 in MOE; 0.37 in the solid state). As a result, the background emission (blue) of **BN** is always dominant, making **BN** ineffective for creating multi-coloured images on a solid substrate using solvents as ink (see Fig. S45b and c†). In fact, **BO-1** is the only molecule that displays full colours on the TLC plates. The highly visible red-orange emission colour of **BO-1** generated by water on a silica gel substrate is certainly unique among the compounds we examined and critical for creating full-coloured paintings on TLC plates. The same approach can also be applied to non-fluorescent paper substrates. However, on filter papers, the dispersed **BO-1** compound emits a weak red colour, which can be switched to bright blue, green or yellow emission colours with writing using solvents such as toluene or DMF, but cannot produce the red colour by writing with water (see Fig. S45d†). The cellulose of the filter paper likely behaves like water and stabilizes the closed form of **BO-1**.

This journal is © The Royal Society of Chemistry 2018

Open Access Article. Published on 04 January 2018. Downloaded on 28/07/2024 1:37:06 AM.
This article is licensed under a Creative Commons Attribution-NonCommercial 3.0 Unported Licence.

Distinct temperature-dependent emission of BO-1

Both **BO-1** and **BO-2** display temperature-dependent emission spectral changes, but with a distinct difference. At 77 K the emission spectrum of **BO-1** is dominated by a red-orange peak, with a notable presence of a blue emission peak at about 450 nm, which could be attributed to the closed and the open form of **BO-1**, respectively. The ratio of the yellow/orange peak *versus* the blue peak is dependent on the solvent and the concentration of **BO-1** at 77 K. Increasing concentration greatly enhances the relative intensity of the yellow/orange peak of **BO-1**. For **BO-2**, its 77 K emission spectrum is almost entirely from the red-orange emission peak. From 77 K to near the melting point of the solvent, the emission peak of **BO-2** loses intensity rapidly (*e.g.* $\Phi_{FL} = \sim 0.02$ from 202 K to 157 K in CH_2Cl_2) and the emission colour shifts from yellow-orange to sky-blue with erratic changes in the CIE coordinates (see Fig. S43†). Above m.p., the emission colour of **BO-2** gradually shifts back to yellow-green with increasing T, accompanied by a gradual increase in emission intensity. Increased ICT character of the *c*-**BO-2** molecule with T may account for its emission intensity gain and bathochromic shift.

In contrast, for **BO-1**, in CH_2Cl_2 (m.p. = 176 K) or MOE (2-methoxyethyl ether, m.p. = 205 K, 0.1 mM), there are two well separated regions in the CIE diagram that display approximately linear changes in CIE coordinates (see Fig. S38(b)†) with T, one below the m.p. and one above the m.p. of the solvent (Fig. 6). Below m.p. (the red region of the emission spectra) the emission colour of **BO-1** changes with increasing T from yellow-orange to blue. In CH_2Cl_2 or MOE, at or near the m.p., the CIE coordinates of **BO-1** undergo a sharp transition from blue to green, which is clearly caused by the phase change of the solvent. Above m.p. (the black region of the emission spectra), the emission peak moves back toward blue and increases intensity with increasing T. The switching of the closed form to the open form is likely a main cause for the emission colour change in the low T region. Variable temperature ^{11}B NMR experiments revealed that the ^{11}B chemical shift of **BO-1** in CD_2Cl_2 is about ~38 ppm at 243 K, near that of **BO-2** (see Fig. S36†), an indication that at 243 K and below, the closed form likely has a major presence in solution. The emission λ_{max} or the ratio of $I_{490\ nm}/I_{525\ nm}$ (see Fig. S38(a)†) of **BO-1** changes linearly and reversibly with T in the region of 223 K to 383 K in MOE, as shown in Fig. 7, an indication that **BO-1** is an effective temperature sensor over a wide temperature range. Because the T-dependent change of the emission spectrum of **BO-1** in MOE at 223–383 K closely resembles that of **BN** (except that **BN** has a steeper slope, compared to that shown in Fig. 7, see Fig. S40–S42 and S44(a)†), the emission colour change of **BO-1** in this temperature region is likely dominated by the donor (amino)–acceptor ICT fluorescence change with T. In solvents such as benzene and hexane (see Fig. S39a and b†), *c*-**BO-1** is more dominant than *o*-**BO-1** at low T. Interestingly, the sharp solvent-phase transition-caused changes in the CIE diagram of **BO-1** in CH_2Cl_2 or MOE were not observed in hexane. Nonetheless, the CIE diagram of **BO-1** in hexane also displays two distinct regions of change, 77 K to 157 K, and 167 K to 298 K. The T-dependent emission colour change of **BO-1** has an excellent reversibility at 223–383 K in MOE, as shown by Fig. 7. In contrast, the emission of **BN** shows a relatively poor reversibility with T under the same conditions (see Fig. S42†).

The high contrast and reversible emission colour change from red/orange to blue/green of **BO-1** over a wide temperature range is unique among the boron compounds examined in this work (**BN** has a deep blue emission colour at low T). Such a sharp contrasting colour change with T is rare for organic dyes. In a recently reported example,[1a] a multidentate Pt(II) chelate compound was shown to switch between monomer phosphorescence (sky-blue, low T) and excimer phosphorescence (red, high T), a trend opposite to that observed for **BO-1**. Compared to the Pt(II) based system, the **BO-1** based system is

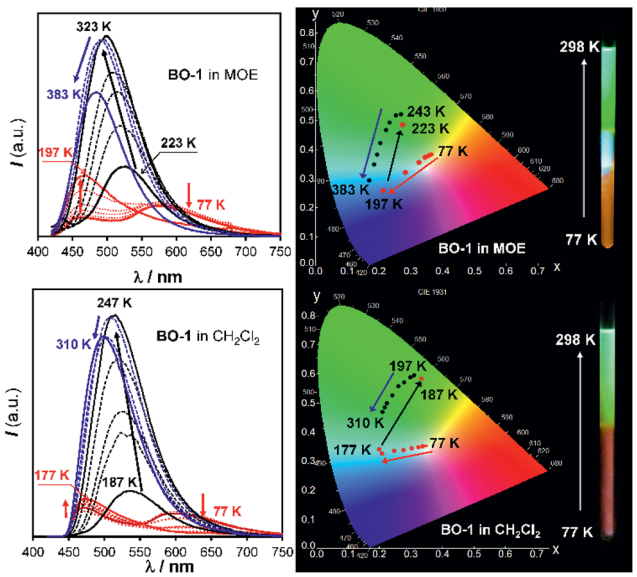

Fig. 6 Emission spectra (left) and CIE coordinate diagrams (right) of **BO-1** in MOE (top) and CH_2Cl_2 (bottom) at various temperatures. Inset: photographs showing the emission colour change of **BO-1** solutions with T in an NMR tube. The bottom half of the NMR tube was cooled to 77 K in liquid nitrogen and the photos were taken immediately after the NMR tube was pulled out of the liquid nitrogen. MOE represents 2-methoxyethyl ether.

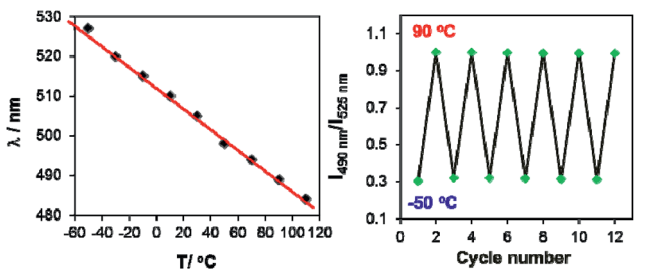

Fig. 7 Left: diagram showing the linear dependence of the emission λ_{max} of **BO-1** fluorescence in MOE on T from 223 K (−50 °C) to 383 K (110 °C). Right: diagram showing the reversible cycling of **BO-1** emission between −50 °C and 90 °C, plotted with the intensity ratio of $I_{490\ nm}/I_{525\ nm}$ *vs.* T.

Open Access Article. Published on 04 January 2018. Downloaded on 28/07/2024 1:37:06 AM.
This article is licensed under a Creative Commons Attribution-NonCommercial 3.0 Unported Licence.

certainly much easier and cheaper to synthesize, and simpler for incorporation into other supporting/functional systems such as polymers for practical temperature sensing applications, which is being investigated in our laboratory.

Emission colour change of BO-1 with pressure

In addition to temperature dependence, the emission spectrum of **BO-1** also displays dependence on pressure. As shown in Fig. 8, upon grinding, the emission peak of **BO-1** powder at 475 nm decreases in intensity and a new peak at ~620 nm appears, which becomes the dominating emission peak with increasing grinding time. As a result, the emission colour of **BO-1** powder changes from whitish blue to red-orange. The red emission band of **BO-1** is in fact similar to those of **BO-2** and **BO-3** in the solid state (Fig. 8). The visual colour of **BO-1** powder also changes from light yellow to orange with grinding. In addition, the amorphous film of **BO-1** produced by casting the **BO-1** solution in organic solvent such as CH_2Cl_2 on a glass substrate also has a red-orange emission band similar to that of the ground powder. Both the ground powder and the film of **BO-1** have a distinct weak absorption band at ~500 nm (see Fig. S30†), resembling those of **BO-2** film/**BO-3** solution/film, and **BO-1** in THF : water solution (1 : 9). IR spectra showed the appearance of a distinct C–O stretching band at 1517 cm^{-1} for the partially ground powder of **BO-1**, which is identical to the strong C–O stretching band of **BO-3** and **BO** powder (see Fig. S48†). Based on these observations, we suggest that the red-orange emission peak of the ground powder and the film of **BO-1** likely originates from *c*-**BO-1**. The ground powder and the amorphous film of **BO-1** can return to the crystalline state at ambient temperature, which can be accelerated with heating, either fully or partially restoring the blue emission peak (Fig. 8). It is possible to create blue and red emission patterns using a spatula to scratch the powder of **BO-1** on a glass surface (see Fig. S45a†).

Force-responsive systems based on boron compounds are very rare. To the best of our knowledge, the only well-established examples are those reported by Fraser and coworkers,[7] which are based on BF_2-chelated α,β-diketonate derivatives and do not involve structural change. Wakamiya and coworkers also recently reported a boron system that changes colour from yellow to green in the solid state upon grinding, and attributed this phenomenon to the change of the dye molecule from a crystalline state to a partially amorphous state.[6a] **BO-1** is a new example of boron-based systems that display a drastic and reversible colour change in response to temperature and pressure.

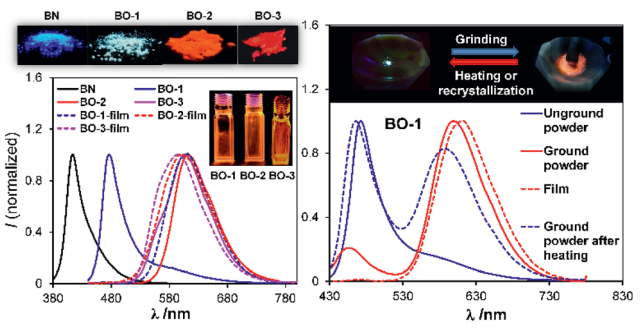

Fig. 8 Left: photographs showing the emission colours of BN, BO-1–BO-3 in the crystalline state and as amorphous films, and the corresponding emission spectra. Right, top: photographs showing the emission colour change of BO-1 powder in a mortar with grinding; bottom: emission spectra of BO-1 in various states.

Conclusions

We have established that the introduction of an *ortho* aldehyde group in proximity to a boron centre in an amino-triarylborane donor–acceptor system allows the achievement of a simple multi-stimuli responsive system, in which the reversible switching of a B ← O bond likely plays a key role. In addition, the imbedded intramolecular donor (amino)–acceptor (boron–aldehyde) charge transfer transition in this system also plays a critical role in modulating the structural switching and the emission colour. This finding introduces new guiding principles in molecular structure design/materials engineering for achieving simple and highly effective multi-responsive systems based on organoboron compounds.

Experimental

General

The THF solvent used for the synthesis of **BO-1**–**BO-3** was freshly distilled over sodium metal and stored under nitrogen prior to use. All other solvents and commercial chemicals were used without further purification. UV-visible absorption spectra were recorded on a Cary 300 UV-Vis spectrophotometer. Fluorescence quantum efficiencies were determined using a Hamamatsu C11347-11 Quantaurus-QY spectrometer. ^{1}H, ^{11}B and ^{13}C NMR spectra were recorded on a Bruker Avance 400 MHz or 700 MHz spectrometer. Luminescence spectra were recorded on an Edinburgh Instruments FLS980 or a Lengguang Tech F97 Pro spectrophotometer. Electrochemical measurements were conducted on an AUTOLAB-CV-75W analyzer with a scan rate of 100 mV s^{-1}. The electrochemical cell was a standard three-compartment cell composed of a Pt working electrode, a Pt auxiliary electrode, and a Pt wire reference electrode. All measurements were performed using 0.10 M of NBu_4PF_6 in DMF as the supporting electrolyte. The potentials are reported relative to the ferrocene/ferrocenium couple. Powder X-ray diffraction patterns were recorded on a Bruker D8 Advance diffractometer. High resolution mass spectral data were obtained *via* ESI on an Agilent (Q-TOF 6520) analyzer. Column chromatography was carried out on silica gel (300–400 mesh). Analytical thin-layer chromatography was performed on glass plates of Silica Gel GF-254. Compounds **BN**[10a] and **BO**[14] were prepared using methods described in the literature. 5-(*N*,*N*-Dimethylamino)-2-bromobenzaldehyde (**1a**) was also prepared according to a literature procedure.[15]

Synthesis of BO-1

Compound **1a** (0.50 g, 2.19 mmol) and triethyl orthoformate (1.2 mL, 7.23 mmol) were dissolved in ethanol (10 mL), and

This journal is © The Royal Society of Chemistry 2018

Open Access Article. Published on 04 January 2018. Downloaded on 28/07/2024 1:37:06 AM. This article is licensed under a Creative Commons Attribution-NonCommercial 3.0 Unported Licence.

then a catalytic amount of concentrated HCl (31 μL) was added. The reaction mixture was refluxed for 4 h. After compound **1a** was completely consumed, the reaction mixture was brought to room temperature, then washed and extracted with water and ethyl acetate, respectively. The combined organic layers were washed with brine and dried over anhydrous Na_2SO_4. After removing the solvents under reduced pressure, compound **1b** was obtained as a colourless liquid (0.65 g, 99% yield). ^{1}H NMR (400 MHz, $CDCl_3$): δ 7.33 (d, J = 8.8 Hz, 1H), 7.01 (d, J = 3.1 Hz, 1H), 6.55 (dd, J = 8.8, 3.1 Hz, 1H), 5.59 (s, 1H), 3.76–3.54 (m, 4H), 2.94 (s, 6H), 1.26 (t, J = 7.0 Hz, 6H) ppm. To an oven-dried Schlenk flask was added **1b** (0.70 g, 2.63 mmol) and the flask was evacuated and back-filled with N_2 three times. THF (10 mL) was then added and the mixture was cooled to −78 °C using an acetone and liquid nitrogen bath. *n*-BuLi (1.8 mL of 1.6 M solution in hexane, 2.89 mmol) was added over 30 min. After 1 h, a solution of Mes_2BF (0.82 g, 2.73 mmol) in 4 mL of THF was added over 10 min. The reaction mixture was warmed to room temperature, and stirring was continued for 12 h. HCl (8 mL, 1 N) was added and stirring was continued for another 4 h. The reaction mixture was then extracted with diethyl ether. The combined organic layers were washed with a brine solution and dried over anhydrous Na_2SO_4. After removing the solvents at reduced pressure, the crude product was purified by silica gel chromatography using petroleum ether and ethyl acetate (20 : 1) as the eluent. Compound **BO-1** was obtained as a yellow solid in 65% yield (0.67 g, 1.70 mmol). ^{1}H NMR (400 MHz, C_6D_6): δ 9.86 (s, 1H), 7.55 (d, J = 8.4 Hz, 1H), 7.24 (d, J = 2.4 Hz, 1H), 6.79 (s, 4H), 6.45 (dd, J = 8.4, 2.4 Hz, 1H), 2.34 (s, 6H), 2.20 (s, 12H), 2.18 (s, 6H) ppm. ^{13}C NMR (176 MHz, CD_3CN): δ 197.19, 152.28, 142.75, 141.32, 137.77, 135.83, 129.55, 119.68, 111.01, 40.39, 23.89, 20.95 ppm. ^{11}B NMR (128 MHz, C_6D_6): δ 60 ppm. HRMS (ESI, m/z): $[M + H]^+$ calcd for $C_{27}H_{33}BNO$, 398.2650; found 398.2662.

Synthesis of BO-2

Compound **2b** was prepared in the same manner as described above for compound **1b**, using compound **2a** (0.25 g, 0.82 mmol), triethyl orthoformate (0.45 mL, 2.71 mmol), ethanol (6 mL), and concentrated HCl (11.89 μL). Compound **2b** was isolated as a white solid (0.28 g, 0.73 mmol, 89%). ^{1}H NMR (400 MHz, $CDCl_3$): δ 7.84 (d, J = 2.4 Hz, 1H), 7.53 (dd, J = 15.6, 8.6 Hz, 3H), 7.37 (dd, J = 8.3, 2.4 Hz, 1H), 6.79 (d, J = 8.8 Hz, 2H), 5.68 (s, 1H), 3.76–3.58 (m, 4H), 3.00 (s, 6H), 1.27 (t, J = 7.1 Hz, 6H). Using **2b** as the starting material (0.25 g, 0.66 mmol), THF (10 mL), *n*-BuLi (0.45 mL of 1.6 M solution in hexane, 0.73 mmol), Mes_2BF (0.22 g, 0.73 mmol), and 2 mL of 1 N HCl, compound **BO-2** was synthesized according to the same procedure as described for **BO-1**. The crude product was purified by silica gel chromatography using CH_2Cl_2 and petroleum ether as the eluent (1 : 1). Compound **BO-2** was obtained as red solid in 64% yield (0.20 g, 0.42 mmol). ^{1}H NMR (400 MHz, C_6D_6): δ 8.59 (s, 1H), 7.88 (d, J = 7.8 Hz, 1H), 7.67 (d, J = 1.2 Hz, 1H), 7.58 (dd, J = 7.8, 1.6 Hz, 1H), 7.46 (d, J = 8.8 Hz, 2H), 6.85 (s, 4H), 6.65 (d, J = 8.8 Hz, 2H), 2.54 (s, 6H), 2.28 (s, 12H), 2.22 (s, 6H) ppm. ^{13}C NMR (176 MHz, $CDCl_3$): δ 196.47, 141.82, 141.01, 139.67, 136.16, 134.36, 133.19, 129.37, 127.92, 125.45, 24.40, 21.03 ppm. ^{11}B NMR (128 MHz, C_6D_6): δ 30 ppm. HRMS (ESI, m/z): $[M + H]^+$ calcd for $C_{33}H_{37}BNO$: 474.2963; found: 474.2966.

Synthesis of BO-3

A Schlenk flask was charged with **3a** (354 mg; 1.46 mmol) and EtOH (7.0 mL) under air, and concentrated HCl (21 μL) was added. The solution was stirred at 100 °C for 4 h. Water (20 mL) and ethyl acetate (60 mL) were added, and the organic phase was separated, washed with water (3 × 20 mL), brine (30 mL), and dried with $MgSO_4$. After the removal of the solvent, the product was dissolved in THF (20 mL). *n*-BuLi (1.6 M solution in hexane, 0.75 mL, 1.2 mmol) was added dropwise at −78 °C. The mixture was stirred for 1 h at −78 °C and $BMes_2F$ in THF (10 mL) was added, the solution was stirred at −78 °C for 1 h, then warmed to room temperature and stirred for 12 h. The HCl (1 mL, 1 M) was added to the mixture, and the solution was stirred at room temperature for 10 min. After the removal of the solvent, purification of the crude product by column chromatography (ethyl acetate/petroleum ether = 1/10) afforded the product as a red solid, 0.30 g, yield: 50%. ^{1}H NMR (400 MHz, C_6D_6): δ 7.87 (d, J = 8.3 Hz, 1H), 7.15 (s, 1H), 6.87 (s, 4H), 6.70 (d, J = 8.3 Hz, 1H), 6.61 (s, 1H), 2.44 (s, 6H), 2.35 (s, 12H), 2.23 (s, 6H), 1.84 (s, 3H) ppm. ^{13}C NMR (176 MHz, C_6D_6): δ 206.81, 149.05, 140.62, 138.43, 133.98, 132.60, 129.73, 127.98, 122.48, 106.38, 39.79, 24.85, 20.69, 19.23 ppm. ^{11}B NMR (225 MHz, C_6D_6): δ 15.61 ppm. HRMS (ESI, m/z): $[M + H]^+$ calcd for $C_{28}H_{34}BNO$, 412.2812; found 412.2804.

Computational study

DFT and TD-DFT calculations were performed using the Gaussian 09 suite of programs[18] on the High Performance Computing Virtual Laboratory (HPCVL) at Queen's University. Geometry optimizations and vertical excitations of all compounds were obtained at the B3LYP[19]/6-31g(d)[20] level of theory and the resulting structures were confirmed to be stationary points through vibrational frequency analysis. Calculated UV/Vis and IR spectra were generated by GaussSum V3.0.[21] The transition state involved in the interconversion of the open **BO-1** and the closed **BO-1** structures was located by scanning the potential energy surface with the ModRedundant option in Gaussian along the boron–oxygen bond length, followed by an optimization. Vibrational frequency analysis contained only one true imaginary frequency, indicating that the transition state optimization was successful. For details, see ESI.†

Single-crystal X-ray diffraction analysis

The crystal data of **BO**, **BO-1**, **BO-2** and **BO-3** were collected on a Bruker D8-Venture diffractometer with Mo-target (λ = 0.71073 Å) at 180 K. Data were processed on a PC with the aid of the Bruker SHELXTL software package[22] and corrected for absorption effects. The crystals of **BO-1**, **BO-2** and **BO-3** belong to the monoclinic space group $P2_1/n$, $C2/c$, and $P2_1/c$, respectively, while the crystals of **BO** belong to the triclinic space group $P\bar{1}$. All non-hydrogen atoms were refined anisotropically. The

Open Access Article. Published on 04 January 2018. Downloaded on 28/07/2024 1:37:06 AM. This article is licensed under a Creative Commons Attribution-NonCommercial 3.0 Unported Licence.

positions of hydrogen atoms were calculated and their contributions in structural factors were included. The details of crystal data, collection parameters and results of analyses are provided in the ESI.† The crystal data of **BO**, **BO-1**, **BO-2** and **BO-3** were deposited to the Cambridge Crystallographic Data Center with deposition numbers of CCDC 1568989 (**BO-1**), 1568988 (**BO-2**), 1585930 (**BO-3**), 1569175 (**BO**).

Conflicts of interest

There are no conflicts to declare.

Acknowledgements

Y. G. S., G. F. H., X. L., N. W., T. P. and S. W. thank the National Natural Science Foundation of China for financial support (grant no. 201501011, 201571017 and 21701011). H. J. L. thanks the Chinese Scholarship Council for graduate scholarship. H. J. L., S. K. M, and S. W. thank the Natural Sciences and Engineering Research Council of Canada for financial support (RGPIN 1193993-2013) and the High-Performance Computing Virtual Laboratory (HPCVL) at Queen's University for the computing facility.

Notes and references

1 (*a*) L. Liu, X. Wang, N. Wang, T. Peng and S. Wang, *Angew. Chem., Int. Ed.*, 2017, **56**, 9160; (*b*) P. Chen, Q. Li, S. Grindy and N. Holten-Andersen, *J. Am. Chem. Soc.*, 2015, **137**, 11590; (*c*) H.-Y. Ku, B. Tong, Y. Chi, H.-C. Kao, C.-C. Yeh, C.-H. Chang and G.-H. Lee, *Dalton Trans.*, 2015, **44**, 8552; (*d*) X. Zhang, J. Y. Wang, J. Ni, L. Y. Zhang and Z. N. Chen, *Inorg. Chem.*, 2012, **51**, 5569; (*e*) D. S. Achilleos and M. Vamvakaki, *Macromolecules*, 2010, **43**, 7073.

2 J. C. Chan, W. H. Lam, H. L. Wong, N. Zhu, W. T. Wong and V. W. Yam, *J. Am. Chem. Soc.*, 2011, **133**, 12690.

3 (*a*) P. Xue, J. Ding, P. Wang and R. Lu, *J. Mater. Chem. C*, 2016, **4**, 6688; (*b*) L. M. Huang, G. M. Tu, Y. Chi, W. Y. Hung, Y. C. Song, M. R. Tseng, P. T. Chou, G. H. Lee, K. T. Wong, S. H. Cheng and W. S. Tsai, *J. Mater. Chem. C*, 2013, **1**, 7582.

4 (*a*) A. Y.-Y. Tam, K. M.-C. Wong and V. W.-W. Yam, *J. Am. Chem. Soc.*, 2009, **131**, 6253; (*b*) K. Nishino, H. Yamamoto, K. Tanaka and Y. Chujo, *Org. Lett.*, 2016, **18**, 4064.

5 Y. Xing, C. Liu, J. H. Xiu and J. Y. Li, *Inorg. Chem.*, 2015, **54**, 7783.

6 (*a*) H. Shimogawa, O. Yoshikawa, Y. Aramaki, M. Murata, A. Wakamiya and Y. Murata, *Chem.–Eur. J.*, 2017, **23**, 3784; (*b*) Y. Cao, J. K. Nagle, M. O. Wolf and B. O. Patrick, *J. Am. Chem. Soc.*, 2015, **137**, 4888; (*c*) N. Kano, J. Yoshino and T. Kawashima, *Org. Lett.*, 2005, **7**, 3909; (*d*) J. Yoshino, N. Kano and T. Kawashima, *Tetrahedron*, 2008, **64**, 7774; (*e*) J. Feng, L. Xiong, S. Wang, S. Li, Y. Li and G. Yang, *Adv. Funct. Mater.*, 2013, **23**, 340; (*f*) J. Feng, K. Tian, D. Hu, S. Wang, S. Li, Y. Zeng, Y. Li and G. Yang, *Angew. Chem., Int. Ed.*, 2011, **50**, 8072; (*g*) Y. L. Rao, H. Amarne, S. B. Zhao, T. M. McCormick, S. Martic, Y. Sun, R. Y. Wang and S. Wang, *J. Am. Chem. Soc.*, 2008, **130**, 12898; (*h*) Y. L. Rao, H. Amarne and S. N. Wang, *Coord. Chem. Rev.*, 2012, **256**, 759; (*i*) J. Wang, B. Jin, N. Wang, T. Peng, X. Li, Y. Luo and S. Wang, *Macromolecules*, 2017, **50**, 4629; (*j*) A. Iida, S. Saito, T. Sasamori and S. Yamaguchi, *Angew. Chem., Int. Ed.*, 2013, **52**, 3760; (*k*) H. Wang, J. Zhang and Z. Xie, *Angew. Chem., Int. Ed.*, 2017, **56**, 9198; (*l*) H. Qian, Y. Y. Wang, D. S. Guo and I. Aprahamian, *J. Am. Chem. Soc.*, 2017, **139**, 1037; (*m*) K. Dhanunjayarao, V. Mukundam and K. Venkatasubbaiah, *Inorg. Chem.*, 2016, **55**, 11153.

7 (*a*) G. Zhang, J. Lu, M. Sabat and C. L. Fraser, *J. Am. Chem. Soc.*, 2010, **132**, 2160; (*b*) G. Zhang, J. P. Singer, S. E. Kooi, R. E. Evans, E. L. Thomas and C. L. Fraser, *J. Mater. Chem.*, 2011, **21**, 8295; (*c*) H. Naito, K. Nishino, Y. Morisaki, K. Tanaka and Y. Chujo, *Angew. Chem., Int. Ed.*, 2017, **56**, 254.

8 (*a*) H. Sohn, M. J. Sailor, D. Magde and W. C. Trogler, *J. Am. Chem. Soc.*, 2003, **125**, 3821; (*b*) Y. Liu, Y. Tang, N. N. Barashkov, I. S. Irgibaeva, J. W. Y. Lam, R. Hu, D. Birimzhanova, Y. Yu and B. Z. Tang, *J. Am. Chem. Soc.*, 2010, **132**, 13951; (*c*) Z. J. Zhao, B. Hea and B. Z. Tang, *Chem. Sci.*, 2015, **6**, 5347; (*d*) J. N. Zhang, H. Kang, N. Li, S. M. Zhou, H. M. Sun, S. W. Yin, N. Zhao and B. Z. Tang, *Chem. Sci.*, 2017, **8**, 577.

9 (*a*) L. Ji, S. Griesbeck and T. B. Marder, *Chem. Sci.*, 2017, **8**, 846; (*b*) F. Jäkle, *Chem. Rev.*, 2010, **110**, 3985; (*c*) C. R. Wade, A. E. J. Broomsgrove, S. Aldridge and F. P. Gabbaï, *Chem. Rev.*, 2010, **110**, 3958; (*d*) Z. M. Hudson and S. Wang, *Acc. Chem. Res.*, 2009, **42**, 1584; (*e*) Y. Shirota and H. Kageyama, *Chem. Rev.*, 2007, **107**, 953; (*f*) C. Reus, S. Weidlich, M. Bolte, H.-W. Lerner and M. Wagner, *J. Am. Chem. Soc.*, 2013, **135**, 12892.

10 (*a*) Z. Yuan, C. D. Entwistle, J. C. Collings, D. Albesa-Jov, A. S. Batsanov, J. A. K. Howard, N. J. Taylor, H. M. Kaiser, D. E. Kaufmann, S.-Y. Poon, W.-Y. Wong, C. Jardin, S. Fathallah, A. Boucekkine, J.-F. Halet and T. B. Marder, *Chem.–Eur. J.*, 2006, **12**, 2758; (*b*) Z. Yuan, J. C. Collings, N. J. Taylor, T. B. Marder, C. Jardin and J.-F. Halet, *J. Solid State Chem.*, 2000, **154**, 5; (*c*) Z. Yuan, N. J. Taylor, Y. Sun, T. B. Marder, I. D. Williams and C. Lap-Tak, *J. Organomet. Chem.*, 1993, **449**, 27; (*d*) Z. Yuan, N. J. Taylor, T. B. Marder, I. D. Williams, S. K. Kurtz and L.-T. Cheng, *J. Chem. Soc., Chem. Commun.*, 1990, 1489.

11 (*a*) P. Chen, R. A. Lalancette and F. Jäkle, *Angew. Chem., Int. Ed.*, 2012, **51**, 7994; (*b*) Y. Kim and F. P. Gabbaï, *J. Am. Chem. Soc.*, 2009, **131**, 3363; (*c*) S. Yamaguchi, S. Akiyama and K. Tamao, *J. Am. Chem. Soc.*, 2001, **123**, 11372; (*d*) X. D. Yin, K. L. Liu, Y. Ren, R. A. Lalancette, Y.-L. Loo and F. Jäkle, *Chem. Sci.*, 2017, **8**, 5497.

12 (*a*) X. Long, Z. Ding, C. Dou, J. Zhang, J. Liu and L. Wang, *Adv. Mater.*, 2016, **28**, 6504; (*b*) C. Dou, X. Long, Z. Ding, Z. Xie, J. Liu and L. Wang, *Angew. Chem., Int. Ed.*, 2016, **55**, 1436; (*c*) R. Zhao, C. Dou, Z. Xie, J. Liu and L. Wang, *Angew. Chem., Int. Ed.*, 2016, **55**, 5313; (*d*) C. Dou, Z. Ding, Z. Zhang, Z. Xie, J. Liu and L. Wang, *Angew. Chem., Int. Ed.*, 2015, **54**, 3648.

13 (*a*) Y. J. Shiu, Y. C. Cheng, W. L. Tsai, C. C. Wu, C. T. Chao, C. W. Lu, Y. Chi, Y. T. Chen, S. H. Liu and P. T. Chou, *Angew.*

 This journal is © The Royal Society of Chemistry 2018

Open Access Article. Published on 04 January 2018. Downloaded on 28/07/2024 1:37:06 AM.
This article is licensed under a Creative Commons Attribution-NonCommercial 3.0 Unported Licence.

Chem., Int. Ed., 2016, **55**, 3017; (*b*) K. Suzuki, S. Kubo, K. Shizu, T. Fukushima, A. Wakamiya, Y. Murata, C. Adachi and H. Kaji, *Angew. Chem., Int. Ed.*, 2015, **54**, 15231; (*c*) H. Hirai, K. Nakajima, S. Nakatsuka, K. Shiren, J. Ni, S. Nomura, T. Ikuta and T. Hatakeyama, *Angew. Chem., Int. Ed.*, 2015, **54**, 13581; (*d*) F. H. Li, W. L. Jia, S. Wang, Y. Q. Zhao and Z. H. Lu, *J. Appl. Phys.*, 2008, **103**, 034509; (*e*) W. L. Jia, X. D. Feng, D. R. Bai, Z. H. Lu, S. Wang and G. Vamvounis, *Chem. Mater.*, 2005, **17**, 164; (*f*) D. L. Crossley, I. A. Cade, E. R. Clark, A. Escande, M. J. Humphries, S. M. King, I. Vitorica-Yrezabal, M. J. Ingleson and M. L. Turner, *Chem. Sci.*, 2015, **6**, 5144.

14 (*a*) B. Neue, R. Fröhlich, B. Wibbeling, A. Fukazawa, A. Wakamiya, S. Yamaguchi and E.-U. Würthwein, *J. Org. Chem.*, 2012, **77**, 2176; (*b*) Z. García-Hernández and F. P. Gabbaï, *Z. Naturforsch.*, 2009, **64b**, 1381.

15 M. Barbasiewicz, M. Michalak and K. Grela, *Chem.–Eur. J.*, 2012, **18**, 14237.

16 (*a*) X. G. Liu, Q. L. Qiao, W. M. Tian, W. J. Liu, J. Chen, M. J. Lang and Z. C. Xu, *J. Am. Chem. Soc.*, 2016, **138**, 6960; (*b*) G. Balkowski, A. Szemik-Hojniak, I. H. M. van Stokkum, H. Zhang and W. J. Buma, *J. Phys. Chem. A*, 2005, **109**, 3535; (*c*) X. G. Liu, J. M. Cole and Z. C. Xu, *J. Phys. Chem. C*, 2017, **121**, 13274.

17 F. A. Carey and R. J. Sundberg, *Advanced Organic Chemistry, Part A: Structure and Mechanism*, Plenum Press, New York, 3rd edn, 1990.

18 M. J. Frisch, G. W. Trucks, H. B. Schlegel, G. E. Scuseria, M. A. Robb, J. R. Cheeseman, G. Scalmani, V. Barone, B. Mennucci, G. A. H. Petersson, M. Nakatsuji, X. Caricato, H. P. F. Li, A. Hratchian, J. Izmaylov, G. Bloino, J. L. Zheng, M. Sonnenberg, M. Hada, K. Ehara, R. Toyota, J. Fukuda, M. Hasegawa, T. Ishida, Y. Nakajima, O. Honda, H. Kitao, T. Nakai, J. A. Vreven, J. E. Montgomery Jr, F. Peralta, M. Ogliaro, J. J. Bearpark, E. Heyd, K. N. Brothers, V. N. Kudin, T. Staroverov, R. Keith, J. Kobayashi, K. Normand, A. Raghavachari, J. C. Rendell, S. S. Burant, J. Iyengar, M. Tomasi, N. Cossi, J. M. Rega, M. Millam, J. E. Klene, J. B. Knox, V. Cross, C. Bakken, J. Adamo, R. Jaramillo, R. E. Gomperts, O. Stratmann, A. J. Yazyev, R. Austin, C. Cammi, J. W. Pomelli, R. L. Ochterski, K. Martin, V. G. Morokuma, G. A. Zakrzewski, P. Voth, J. J. Salvador, S. Dannenberg, A. D. Dapprich, O. Daniels, J. B. Farkas, J. V. Foresman, J. Ortiz, J. Cioslowski and D. J. Fox, *Gaussian 09 Revision C.01*, 2010.

19 T. Yanai, D. Tew and N. Handy, *Chem. Phys. Lett.*, 2004, **393**, 51.

20 (*a*) R. Ditchfield, W. J. Hehre and J. A. Pople, *J. Chem. Phys.*, 1971, **54**, 724; (*b*) A. D. McLean and G. S. Chandler, *J. Chem. Phys.*, 1980, **72**, 5639.

21 N. M. O'Boyle, A. L. Tenderholt and K. M. Langner, *J. Comput. Chem.*, 2008, **29**, 839.

22 *SHELXTL, version 6.14*; Bruker AXS, Madison, WI, 2000–2003.